Adaptation of actin dynamics and membrane tension control for yeast endocytosis

J. Lemière[a, b], J. Berro[a, b, c, §]

[a] Department of Molecular Biophysics and Biochemistry, Nanobiology Institute, Yale University, New Haven, CT, USA
[b] Nanobiology Institute, Yale University, West Haven, CT 06516, USA
[c] Department of Cell Biology, Yale University School of Medicine, New Haven, CT 06520, USA
[§] Contact: julien.berro@yale.edu

Abstract

During clathrin-mediated endocytosis in eukaryotes, actin assembly is required to overcome large membrane tension and turgor pressure. However, the molecular mechanisms that enable the actin machinery to adapt to varying membrane tension remain unclear. Here, we used quantitative microscopy to determine that, upon increased membrane tension, the endocytic machinery of fission yeast cells rapidly adapts by assembling larger amounts of actin. We also demonstrate that cells rapidly reduce their membrane tension using three parallel mechanisms. In addition to the mechanical protection of their cell wall, yeast cells' eisosomes regulate moderate changes in membrane tension on a minute time scale. Meanwhile, a temporary reduction of the number of endocytic events for 2 to 6 minutes allows cells to add large pools of membrane to the plasma membrane. Our study sheds light on the tight connection between membrane tension regulation and endocytosis in yeast, which are likely conserved among eukaryotes.

Introduction

During clathrin-mediated-endocytosis (CME), the cell plasma membrane undergoes a dramatic change in topology to form an invagination that is subsequently pinched off into a vesicle. During this process, the endocytic machinery has to overcome the forces produced by membrane tension and the osmotic pressure that oppose membrane deformation and engulfment. In yeast, these resisting forces are particularly large because their internal turgor pressure is high, ranging from ~0.6 MPa for *Saccharomyces cerevisiae* to ~1 MPa for *Schizosaccharomyces pombe* [1,2]. Consequently the formation of a vesicle requires several thousands of pN [3].

Previous studies have shown that actin dynamics are required for productive endocytosis in yeast [4–7] and in mammalians cells when membrane tension is high [8–10], or when membrane scission proteins are absent [11]. Actin assembly at the endocytic site is believed to provide the forces that overcome turgor pressure and membrane tension to deform the plasma membrane, but the precise mechanisms of force production remain unknown. We also lack a quantitative understanding of the regulation of actin dynamics in response to membrane tension and turgor pressure changes. We expect that a better quantitative characterization of this response will allow us to infer the molecular mechanisms of force production and force sensing during clathrin-mediated endocytosis.

In this study, we applied hypotonic shocks to fission yeast cells to determine how the actin machinery responds to increased membrane tension and turgor pressure during clathrin-mediated endocytosis. After a hypotonic shock, the difference in osmolarity inside and outside the cell instantaneously increases the turgor pressure and the membrane tension. Since cell membranes are virtually unstretchable, yeast cells must adapt their membrane tension while they let water flow inward to equilibrate their cytosol osmolarity to the new environement[12–14].

The mechanisms by which membrane tension is regulated are not fully understood. The yeast cell wall is believed to buffer abrupt changes in turgor pressure

thanks to its high stiffness of ~50 MPa [15]. In addition, similarly to mammalian cells' caveolae which change shape or disassemble in response to increased membrane tension, yeast eisosomes can also disassemble when cells without a cell wall, called protoplasts, are placed in low osmolarity media [16,17]. However, it remains unknown how eisosomes may regulate plasma membrane tension in intact cells, and whether eisosome disassembly directly influences cellular processes such as CME.

Fission yeast is an ideal model system to quantitatively study the regulation mechanisms of membrane tension and its influence on the endocytic machinery. First, because yeast turgor pressure is high, actin is required for CME. Secondly, contrary to mammalian cells, yeast cells are devoid of any adhesion machinery or actin cortex, which usually complicates membrane tension manipulation and result interpretation. Last, quantitative microscopy methods developed in fission yeast are able to uncover fine regulations of the endocytic machinery [18,19].

To probe the contribution of each possible mechanisms of membrane tension regulation and their influence on CME, we submitted yeast cells with or without a cell wall to different hypotonic shocks. Using quantitative fluorescence microscopy, we showed that, on the one hand, actin assembly adapts to increased membrane tension to allow endocytosis to proceed, and, on the other hand, yeast cells rapidly reduce their membrane tension by a) disassembling eisosomes and b) regulating the number of endocytic events that are performed at a given time.

Results

Clathrin-mediated endocytosis in wild-type walled cells is robust over a wide range of chronic and acute changes in media osmolarity

To monitor actin dynamics during clathrin-mediated endocytosis, we imaged fission yeast cells expressing the actin filament crosslinking protein fimbrin (Fim1p) tagged with a monomeric enhanced green fluorescent protein (mEGFP), hereafter called Fim1p-mEGFP (Figure 1A, 1B and 1C). We optimized our imaging protocols, and improved tracking tools and temporal super-resolution alignment methods [18] to a) easily collect hundreds of endocytic events in an unbiased manner and b) achieve high reproducibility between different samples, fields of view and days of experiment (Figure 1D, 1E). These improvements in our quantitative microscopy protocol allow us to detect small differences between mutants or conditions that would be missed with previous methods. We confirmed that Fim1p accumulates to endocytic sites for about 10 seconds, then disassembles while the vesicle diffuses away from the plasma membrane (Figure 1D, 1E) [20,21]. As a convention, the peak of Fim1p is set to time 0 s and corresponds to vesicle scission in intact wild-type cells. In the rest of the paper, intact cells with a cell wall will be referred to as “walled cells”, and cells devoid of a cell wall will be referred to as “protoplasts”.

We aimed to increase the tension of cells’ plasma membrane by rapidly reducing media osmolarity, referred to as acute hypotonic shock. To prevent artifacts due to nutrient concentration changes, we supplemented Edinburgh Minimum Media (EMM5S) with varying sorbitol concentrations (0 to 1.2 M). Before performing hypotonic shocks, we exposed cells to this media for more than 15 minutes. In the rest of the paper, we will refer to this experimental condition as steady state at X M or chronic exposure to X M sorbitol, where X is the sorbitol concentration. To perform acute hypotonic shocks, we used a microfluidic system to rapidly exchange the steady state media with media containing a lower sorbitol concentration, hereafter noted ΔP=-Y M where Y is the difference in media osmolarity (note that the pressure P^* in Pascal is related to P in Molar as $P^* = P \cdot RT \sim 2.45 \cdot 10^6 \cdot P$, where R is the gas constant and T the absolute temperature) (Figure 2A). For all tested osmolarities at steady state in walled wild-type cells, we observed no significant differences in the dynamics of fimbrin recruitment or disassembly, maximum molecule number or endocytic patch movements (Figure 2B). Our results indicate that wild-type walled cells have adaptation mechanisms for chronic exposure to a wide range of osmolarities, which allows them to perform CME in a highly reproducible manner.

We then tested the robustness of the endocytic actin machinery when cells experienced a hypotonic shock, which aimed to abruptly increase the tension of their plasma membrane. To observe the highest possible effect, we imaged cells grown at steady state in 1.2 M sorbitol and rapidly exchanged the media with a buffer free of sorbitol (Figure 2A and 2E), therefore performing an acute hypotonic shock of ΔP=-1.2 M. Despite the high hypotonic shock, which represents a ~3 MPa drop in pressure, CME proceeded quite similarly to steady state conditions (Figure 2C, 2D and 2E). The maximum number of fimbrin proteins was the same before and after the hypotonic shock, but fimbrin assembly and disassembly were 15% faster after the shock. This difference in timing decreased over time to reach respectively 13% and 11% after 6 and 8 minutes, showing that the adaptation to steady state was not fully completed (Figure 2E).

Eisosomes mitigate the response of the endocytic machinery to acute and chronic changes in media osmolarity

The robustness of the endocytic process under a wide range of chronic and acute exposure to different media osmolarity suggests that fission yeast has mechanisms that rapidly regulate plasma membrane tension. Previous studies proposed that eisosomes, furrows at the inner surface of the plasma membrane, have a mechanoprotective role under increased membrane tension in fungi, similar to the protective role of caveolae in endothelial cells [16,17,22–24]. Because loss of Pil1p, the core eisosome component, is sufficient to prevent eisosome assembly [25–27], we repeated our experiments in cells lacking the gene coding for Pil1p (*pil1Δ*) (Figure 3).

Dynamics of Fim1p during CME for wild-type and *pil1Δ* walled cells at steady state in media free of sorbitol were identical (Supplemental Figure S1). However, at steady state in media with high sorbitol concentration, cells lacking eisosomes recruited slightly fewer fimbrin molecules to endocytic patches than wild-type cells (Figure 3A and B). The maximum number of Fim1p assembled at CME sites in *pil1Δ* cells in buffer containing 0.8 M and 1.2 M sorbitol was 10% and 17% lower, respectively. Within the first two minutes of an acute hypotonic shock from 1.2 M sorbitol to 0 M (ΔP=-1.2 M), the maximum number of Fim1p increased by 30%, while its timing was shortened by 30% compared to steady-state (Figure 3C & 3D). Four minutes after the hypotonic shock, the dynamics of fimbrin stabilized to its steady state dynamics in 0 M sorbitol (Figure 3B & 3D). Overall, our data show that cells lacking eisosomes are more sensitive than wild-type cells to acute and chronic changes in media osmolarity.

Eisosomes participate in the regulation of protoplasts' membrane tension during hypotonic shocks

The yeast cell wall plays a role in the maintenance of cell integrity under extreme conditions, thanks to its high stiffness of ~50 MPa [15]. We hypothesized that the cell wall prevents large variations in membrane tension under hypotonic shocks, which would explain why endocytosis in wild-type walled cells remains virtually unchanged in the extreme conditions we tested (Figure 2E). Hence, to exclude the effect of the cell wall, we reiterated our experiments using protoplasts instead of intact cells.

First, we characterized how the removal of the cell wall affects eisosomes' reorganization and CME. We used a preparation protocol that allowed us to manipulate protoplasts for up to ~1 hour after their formation, since they remain void of cell wall for about 3 hours [28]. Because protoplasts are more fragile than walled cells, they were prepared in media containing 0.25 to 1.2 M sorbitol to balance turgor pressure and prevent cells from bursting [5,17,29], and were imaged ~15 minutes later, once they reached steady state.

Our data show that endocytic patches and eisosomes in protoplasts at steady state in 1.2 M sorbitol are qualitatively similar to those in walled cells (Figure 4A). However, the surface area of the protoplasts' plasma membrane covered by eisosomes decreased with decreasing media osmolarity at steady state (Figure 4B and 4C), and correlated with increasing cell volume. This result suggests that eisosomes might be disassembled to reduce membrane tension in media with low osmolarity.

To test whether membrane tension is indeed buffered by eisosomes, we measured membrane tension using a micropipette aspiration assay (Figure 4D). At steady state in 0.8 M sorbitol, the membrane tension was 4.5±1.4 10^{-4} nN·µm^{-1} for wild-type protoplasts and 3.9±1.3 10^{-4} nN·µm^{-1} for *pil1Δ* protoplasts (Figure 4E). We then reproduced these measurements within 5 minutes after inducing a hypotonic shock of ΔP=-0.2 M. We observed a 1.6-fold increase in membrane tension for wild-type

protoplasts (7.3±2.1 10^{-4} nN·µm^{-1}) and a 4.5-fold increase for protoplasts lacking eisosomes (17.4±6.1 10^{-4} nN·µm^{-1}). This result demonstrates that eisosomes participate in the adjustment of cell membrane tension.

CME in protoplasts is sensitive to chronic changes in osmolarity

Endocytosis in wild-type protoplasts at steady state in medium containing 0.4 or 0.8 M sorbitol was able to proceed normally by recruiting almost the same number of fimbrin molecules as in walled cells, but with a slightly longer timing (Figure 4F). In contrast, in medium with 1.2 M sorbitol, the timing of fimbrin recruitment was dramatically longer, and endocytosis failed to proceed normally, as reported by the virtually null speed of patches during the entire time fimbrin is present at the endocytic site (Figure 4F). Cells lacking eisosomes showed very similar phenotypes but endocytosis started failing at 0.8 M sorbitol (Figure 4G).

At 0.25 M sorbitol, both wild-type and *pil1Δ* protoplasts were able to perform endocytosis but required a larger amount of Fim1p (Figure 4F and 4G). In these conditions, the eisosomes covered only half of the plasma membrane surface area they cover at 0.4M sorbitol (Figure 4B and C) and our data suggest the plasma membrane was highly stretched (Figure 4E). This result indicates that during CME the actin machinery is able to adapt to mechanical cues by mechanisms that are independent of the cell wall.

For both wild-type and *pil1Δ* protoplasts in 0.4 M sorbitol, the temporal evolution of the number of fimbrin molecules and the speed of patches were close to the same metrics measured in walled cells in media without sorbitol (Figure 4F and 4G). These results suggest that the osmotic pressure at these concentrations, which are equivalent to a pressure of 1 MPa, is close to the naturally maintained turgor pressure of walled fission yeast cells, in good agreement with previous measurements [2]. Therefore, to keep our protoplasts in conditions as close to walled cells as possible, the steady state media used in our following experiments on protoplasts contained 0.4 M sorbitol.

In protoplasts, eisosomes buffer moderate hypotonic shocks, and the endocytic actin machinery rapidly adapts to increases in membrane tension

To characterize the adaptation of the endocytic actin machinery to a rapid increase in turgor pressure and membrane tension, we repeated our acute hypotonic shocks (ΔP=-0.05 M, -0.1 M or -0.2 M) on protoplasts initially at steady state in media containing 0.4 M sorbitol. After low (ΔP=-0.05 M) and medium (ΔP=-0.1 M) acute shocks in wild-type protoplasts, we did not observe any stalled endocytic events – when cells started the recruitment of the actin machinery, endocytosis proceeded to successful completion (Figure 5A, 5B and Supplemental Figure S2A). The recruitment of fimbrin did not significantly change over time. In contrast, two minutes after a ΔP=-0.2 M shock, endocytic sites recruited 20% more fimbrin and took 23% more time to perform endocytosis (Figure 5C, 5D, and Supplemental Figure S2A). The actin machinery recovered its steady state behavior less than 4 minutes after the shock (Figure 5D).

We repeated these experiments with *pil1Δ* protoplasts to eliminate the role of eisosomes in the reduction of membrane tension during hypotonic shocks. Immediately (0 minutes) after the lowest hypotonic shock tested (ΔP=-0.05 M), fimbrin recruitment took slightly longer and the number of proteins recruited was higher than at steady state (Figure 5E, 5F and 5G, Supplemental Figure S2B). While fimbrin recovered its steady-state dynamics in less than 4 minutes after high acute hypotonic shock (ΔP=-0.2 M) in wild-type protoplasts (Figure 5D), recovery of fimbrin dynamics

to its steady state behavior in *pil1Δ* protoplasts occurred over 10 minutes, even for the most modest hypotonic shock, ΔP=-0.05 M (Figure 5G). The changes in fimbrin dynamics in *pil1Δ* protoplasts became increasingly larger for ΔP=-0.1 M and ΔP=-0.2 M hypotonic shocks – endocytic sites assembled a peak number of fimbrin respectively 24% and 48% larger and took 85% and 53% longer. In addition, most cells were unable to survive more than two minutes after these high hypotonic shocks (Supplemental Figure S3), which prevented us from determining how the actin machinery recovers after large hypotonic shocks in *pil1Δ* protoplasts.

Given that wild-type protoplasts at steady state in 0.25 M sorbitol contain significantly fewer assembled eisosomes despite expressing normal amounts of Pil1p (Figure 4B and 4C), we took advantage of this condition to further test the role of eisosomes in buffering membrane tension during an acute hypotonic shock and to distinguish the role of eisosomes from the role of unassembled Pil1p proteins. We submitted wild-type protoplasts at steady state in 0.25 M sorbitol to an acute hypotonic shock of ΔP=-0.1 M (Figure 5H and 5I). Two minutes after the shock, endocytic sites accumulated 73% more fimbrin and took 60% longer (Figure 5H, Supplemental Figure S4A). This behavior was nearly identical to fimbrin dynamics in *pil1Δ* protoplasts under the same conditions (Figure 5I, Supplemental Figure S4B). Moreover, most wild-type and *pil1Δ* protoplasts were unable to survive longer than 4 minutes after these high hypotonic shocks (Supplemental Figure S5). This result further demonstrates that the presence of assembled eisosomes at the plasma membrane is indeed responsible for the adaptation of cells to acute hypotonic shocks, and the presence of Pil1p in the cytoplasm is not sufficient for this response.

Altogether, this series of experiments demonstrates that a) eisosomes protect protoplasts from changes in their membrane tension, but only to a certain extent, b) without eisosomes, protoplasts can withstand only minor changes in their membrane tension, c) the endocytic actin machinery adapts to compensate the increase in membrane tension, and d) actin dynamics recovers its steady state dynamics within a few minutes, providing the protoplasts survive the hypotonic shock.

Membrane tension and eisosomes modulate the number of endocytic events in cells

The fast recovery of the actin machinery after an acute change in turgor pressure and membrane tension is surprising and cannot be explained by the sole release of membrane via eisosome disassembly (Figure 5H and 5I). We hypothesized that a decrease in the number of endocytic events happening in the cell at a given time would gradually increase the surface area of the plasma membrane, and therefore reduce membrane tension. We measured the endocytic density, i.e. the number of endocytic events in a cell normalized by the cell length, in wild-type and *pil1Δ* cells after a hypotonic shock using the ratiometric method developed in [19]. For all shocks tested in wild-type (ΔP=-0.05 M, -0.1 M, -0.2 M) and *pil1Δ* protoplasts (ΔP=-0.025 M, -0.05 M, -0.1 M) initially at steady state in 0.4 M sorbitol, the endocytic density in protoplasts significantly decreased immediately after the hypotonic shock (Figure 6A). The difference increased for increasing hypotonic shocks, up to 36% for wild-type protoplasts after a ΔP=-0.2 M shock, and 79% for *pil1Δ* protoplasts after a ΔP=-0.1 M shock (Figure 6B). These abrupt changes in the endocytic density were followed by a 2- to 6-minute recovery back to the steady-state endocytic density, and recovery time depended on the magnitude of the hypotonic shock. The temporal variations of the endocytic density after hypotonic shocks mirrored the changes in Fim1p dynamics in

endocytic patches in similar conditions (Figure 5C, 5D, 5F and 5G). The change in cell volume (Figure 6A & 6B, insets) could not exclusively account for the observed decrease in the endocytic density as the volume increased faster than the change in endocytic density.

Building on these results in protoplasts, we wondered whether the endocytic density in walled cells also adapts to hypotonic shocks. Indeed, immediately after the largest shock tested (ΔP=-1.2 M), we observed a similar decrease in the endocytic density for both wild-type and *pil1⊿* walled cells, 36% and 46% respectively (Figure 6C). Recovery to steady-state endocytic densities occurred in less than 2 minutes in both wild-type and *pil1⊿* walled cells, faster than in protoplasts (Figure 6A, 6B and 6C). These results were surprising because we detected virtually no difference in the dynamics of fimbrin recruitment to endocytic sites in both strains (Figure 2E). Our data show that the cell wall limits but does not completely cancel the effect of hypotonic shocks. They also suggest that the regulation of the endocytic density supplements the regulation performed by the eisosomes to reduce membrane tension and enable normal actin machinery dynamics at endocytic sites.

Wild-type and *pil1⊿* walled cells had a very similar adaptation after hypotonic shocks. However, we noticed a difference in the endocytic density at steady state in different sorbitol concentrations. For all concentrations tested (0 to 2 M), wild-type cells maintained roughly the same endocytic density. In contrast, the steady state endocytic density in *pil1⊿* cells increased with increasing media osmolarity, up to 56% in 2 M sorbitol (Figure 6D). Our results suggest that eisosomes participate in maintaining a constant density of endocytosis independently of the media osmolarity, not only after an abrupt change in membrane tension, but also when they are at steady state in different osmolarity.

Discussion

Robustness of CME in fission yeast

Our data demonstrate that CME is able to proceed in a wide variety of conditions of osmolarities and membrane tension. Even cells devoid of a cell wall and eisosomes were able to perform endocytosis after an acute change in membrane tension, as long as their plasma membrane was not damaged and cells remained alive. Even in the most extreme conditions tested, i.e. cells devoid of a cell wall and lacking the majority of their eisosomes, the dynamics of fimbrin at endocytic sites was only two times larger than what was observed in wild-type walled cells. These results demonstrate that not only are cells able to adapt their endocytic machinery to acute changes in membrane tension but, they are also able to rapidly regulate their membrane tension.

Mechanisms of tension regulation and homeostasis of the plasma membrane

Our results demonstrate that the regulation of membrane tension is performed via a combination of three mechanisms: mechanical protection by the cell wall, disassembly of the eisosomes and temporary reduction of the rate of endocytosis. Our data indicate that all three mechanisms are used in parallel, since wild-type walled cells are less sensitive to acute hypotonic shocks than wild-type protoplasts and *pil1Δ* walled cells, and they experience a temporary decrease in their endocytic density for about 2 minutes after the shock. In addition, our data allow us to estimate the relative contribution of each mechanism in the regulation of membrane tension.

The cell wall provides the highest protection during chronic and acute changes in media osmolarity. Wild-type walled cells are virtually insensitive to osmotic changes, and *pil1Δ* walled cells are much less sensitive than *pil1Δ* protoplasts. Removal of the cell wall dramatically affects actin dynamics at endocytic sites and eisosome assembly at the plasma membrane (Figure 4B, 4C, 4F and 4G). It is surprising that endocytosis in protoplasts still proceeds in media with osmolarity as low as 0.25 M, where most eisosomes are disassembled. In fact, the actin endocytic machinery can overcome membrane tensions high enough to rupture the plasma membrane.

Our results add to a growing body of evidence that eisosomes play a critical role in the regulation of membrane tension and membrane integrity through dynamic remodeling and scaffolding of the plasma membrane. Wild-type walled cells are not sensitive to chronic or acute hypotonic changes, whereas *pil1Δ* walled cells are. The protective role of eisosomes is even more striking in protoplasts under acute hypotonic shocks. Wild-type protoplasts whose plasma membrane is covered with eisosomes are largely insensitive to increases in membrane tension whereas protoplasts with little to no eisosomes are extremely sensitive to increases in membrane tension and their plasma membrane is easily damaged. Our micropipette aspiration experiments also demonstrate that eisosomes are critical to keep membrane tension low during an acute hypotonic shock. Therefore, our data indicate that membrane tension is decreased via the disassembly of eisosomes, through release of excess membrane surface area. Assuming eisosomes are hemi-cylinders with diameter ~50 nm and cells contain 1.6 μm of eisosomes per μm^2 of plasma membrane on average, total eisosome disassembly could release about 5% of the total surface area of the plasma membrane over ~3 minutes after a hypotonic shock [17]. Recent single-molecule imaging in our lab demonstrated that at steady state Pil1p undergoes rapid exchange at the eisosome ends [30], potentially providing a convenient route for rapid disassembly of the BAR domain-mediated scaffold, analogous to filament depolymerization.

Our study identified a third, new mechanism to reduce membrane tension by temporarily reducing the endocytic density. Using our data and previous measurements [18,19], we estimate that cells endocytose about 2% of their surface area per minute. Assuming that at steady state the surface area added to the plasma membrane via exocytosis balances the surface area that is endocytosed, a reduction of the endocytic rate while keeping the exocytic rate constant for a few minutes would allow for a net addition of surface area to the plasma membrane. For example, in *pil1Δ* protoplasts initially at steady state in 0.4 M sorbitol the endocytic rate is reduced by ~25 % for ~10 minutes after an acute hypotonic shock of ΔP=-0.05 M. The net surface area added over that period corresponds to a 5% increase in the protoplast surface area, while the protoplast surface area increased by ~12% over the same period. These estimates demonstrate that modulating the rate of endocytosis is an efficient way to increase the surface area of the plasma membrane by large amounts but this process is relatively slow compared to eisosome disassembly. The slowness of this process might explain why *pil1Δ* and pre-stretched wild-type protoplasts that have about half the normal amount of eisosomes on their surface do not survive even relatively small hypotonic shocks, being unable to provide enough membrane in a short amount of time to reduce the tension of their plasma membrane.

Molecular mechanisms driving the adaptation of the actin endocytic machinery and the rate of endocytosis under various membrane tensions

Under conditions where membrane tension and turgor pressure were significantly increased, we observed that the endocytic actin machinery took longer

and assembled a larger number of fimbrin molecules to successfully produce endocytic vesicles. This effect increased with increasing membrane tension, up to tensions high enough to rupture the cell plasma membrane. This result strongly supports the idea that the actin machinery provides the force that counteracts membrane tension and turgor pressure and deforms the plasma membrane into an endocytic pit.

The precise molecular mechanism that regulates this enhanced assembly remains to be uncovered. Our data suggest that actin dynamics is controlled via a mechanical or geometrical regulation, where actin assembles until the plasma membrane is deformed and pinched off. An alternative, and non-mutually exclusive, hypothesis is that the activity and/or recruitment of proteins upstream of the actin nucleators may be enhanced by increased membrane tension. A third hypothesis is that the decrease in the number of endocytic events after an increase in membrane tension leads to an increase in the concentration of endocytic proteins in the cytoplasm, which can then enhance the reactions performed at the endocytic sites. Sirotkin et al (2010)[21] measured that 65% to 85% of the total cellular content of key proteins involved in the endocytic actin machinery are localized to endocytic sites at any time. A 20% decrease in the number of endocytic sites would increase their cytoplasmic abundance by roughly 40% to 80%. This percentage is larger than the volume changes we measured, resulting in a net increase in the cytoplasmic concentration of these proteins, which would allow larger amount of protein to assemble at the endocytic sites.

Conversely, the decreased rate of endocytic events could be attributed to the larger number of endocytic proteins assembled at each endocytic sites, which would decrease their cytoplasmic concentration. Indeed, Burke *et al*. [31] showed that modulating actin concentration modulates the number of endocytic sites in the same direction. However, it is more likely that one or several early endocytic proteins are sensitive to membrane tension, and either fail to bind the plasma membrane or prevent the triggering of actin assembly when membrane tension is high. This idea would be consistent with results from mammalian cells demonstrating that the proportion of stalled clathrin-coated pits increases when membrane tension increases [32]. In addition, several endocytic proteins that arrive before or concomitantly with the activators of the actin machinery contain BAR domains (such as Syp1p, Bzz1p and Cdc15p), and other members of this domain family (which also includes Pil1) have been shown to bind membranes in a tension-sensitive manner. Further quantitative study of early endocytic proteins will help uncover the validity and relative contributions of each one of these hypotheses.

We expect our results are relevant to the study of CME and membrane tension regulation in higher order eukaryotes. Indeed, the molecular machineries for endocytosis, exocytosis and osmotic response are highly conserved between fission yeast and other eukaryotes. In addition, regulation of membrane tension and CME are particularly critical during cell polarization [33], during neuron development and shape changes [34] and at synapses where large pools of membranes are added and retrieved on a very fast time scale [35,36].

Materials and Methods

Yeast strains and media

The *S. pombe* strains used in this study are listed in Supplemental Table S1. Yeast cells were grown in YE5S (Yeast Extract supplemented with 0.225 g/L of uracil, lysine, histidine, adenine and leucine), which was supplemented with 0 to 1.2 M D-Sorbitol, at 32°C in exponential phase for about 18 hours. Cells were washed twice and resuspended in filtered EMM5S (Edinburgh Minimum media supplemented with 0.225 g/L of uracil, lysine, histidine, adenine and leucine), which was supplemented with the same concentration of D-Sorbitol, at least 10 minutes before imaging so they can adapt and reach steady state.

Protoplasts preparation

S. pombe cells were grown in YE5S at 32°C in exponential phase for about 18 hours. 10 mL of cells were harvested and washed two times with SCS buffer (20 mM citrate buffer, 1 M D-Sorbitol, pH=5.8), and resuspended in SCS supplemented with 0.1 g/mL Lallzyme (Lallemand, Montreal, Canada) [28]. Cells were incubated with gentle shaking for 10 minutes at 37°C in the dark. The resulting protoplasts were gently washed twice in EMM5S with 0.25 to 1.2 M D-Sorbitol, spun down for 3 minutes at 0.4 rcf between washes, and resuspended in EMM5S buffer supplemented with 0.25 to 1.2 M D-Sorbitol at least 10 minutes before imaging so they can adapt and reach steady state.

Microscopy

Microscopy was performed using a spinning disk confocal microscope, built on a TiE inverted microscope (Nikon, Tokyo, Japan), equipped with a CSU-W1 spinning head (Yokogawa Electric Corporation, Tokyo, Japan), a 100X/1.45NA Phase objective, an iXon Ultra888 EMCCD camera (Andor, Belfast, UK), and the NIS-Elements software v. 4.30.02 (Nikon, Tokyo, Japan) on. The full system was switched on at least 45 minutes prior to any experiments to stabilize the laser power and the room temperature. Cells were loaded into commercially available microfluidics chambers for haploid yeast cells (Y04C-02-5PK, Millipore-Sigma, Saint-Louis, USA) for the CellASIC ONIX2 microfluidics system (Millipore-Sigma, Saint-Louis, USA). Each field of view was imaged for 60 seconds, and each second a stack of 6 z-slices separated by 0.5 µm was imaged. The microscope was focused such that the part of the cell closest to the coverslip was captured.

Acute hypotonic shocks

Walled cells or protoplasts were first imaged in their steady state media (EMM5S supplemented with 0 to 1.2 M D-Sorbitol). The steady state media was exchanged with media supplemented with a lower D-Sorbitol concentration (the concentration difference is noted ΔP), with inlet pressure of 5 psi. This hypotonic shock media was labelled with 6.7 µg/mL of sulforhodamine B (MP Biomedicals LLC, Santa Ana, USA), a red cell-impermeable dye that allowed us to a) monitor the full exchange of the solution in the microfluidic chamber prior to image acquisition, and b) monitor the plasma membrane integrity of the cells after the shock. In each condition, the first movie was started when the sulforhodamine B dye was visible in the field of view. For clarity, this time point is labelled t=0 min in all our figures, but note that we estimate it may vary by up to ~30 seconds between movies and conditions. We imaged cells by

taking one stack of 6 Z-slices per second for 60 seconds. After the end of each movie, we rapidly changed field of view and restarted acquisition one minute after the end of the previous movie, so that movies started every 2 minutes after the acute hypotonic shock. Tracks from cells that contained red fluorescence from the sulforhodamine B dye were excluded from the analysis, because this indicated that cell membrane had been damaged.

Measurement of the temporal evolution of the number of proteins and speed

Movies were processed and analyzed using an updated version of the PatchTrackingTools toolset for the Fiji [37] distribution of ImageJ [18,38]. This new version includes automatic patch tracking capabilities based on the Trackmate library [39], and is available on the Berro lab website: http://campuspress.yale.edu/berrolab/publications/software/. Prior to any quantitative measurements, we corrected our movies for uneven illumination and camera noise. The uneven illumination was measured by imaging a solution of Alexa 488 dye and the camera noise was measured by imaging a field of view with 0% laser power. We tracked Fim1-mEGFP spots with a circular 7-pixel diameter region of interest (ROI), and measured the temporal evolution of the fluorescence intensities and the position of the centers of mass. The spot intensity was corrected for cytoplasmic background using a 9-pixel median filter, and was then corrected for photobleaching. The photobleaching rate was estimated by fitting a single exponential to the temporal evolution of the intensity of cytoplasmic ROIs void of any identifiable spots of fluorescence [18]. Only tracks longer than 5 s and displaying an increase followed by a decrease in intensity were kept for the analysis. Individual tracks were aligned and averaged with the temporal super-resolution algorithm from [18], and post-processed using custom scripts in Matlab R2016a (Mathworks). To control and calibrate the intensity of our measurements, we imaged wild-type walled cell expressing Fim1p-mEGP each imaging day. Intensities were converted into number of molecules with a calibration factor such that the peak intensity of our control strain corresponded to 830 molecules [19].

Measurement of the density of CME events

We used the *S. Pombe* profiling tools for ImageJ [18] to measure the number of endocytic events at a given time in each cell. In brief, on a sum-projected z-stack, we manually outlined individual cells, and, for each position along the long axis of a cell, we measured the sum of fluorescence orthogonal to the long axis. We corrected the intensity profile in each cell for its cytoplasmic intensity and media fluorescence outside the cell. We estimated the number of patches in each cell by dividing the corrected fluorescence signal with the temporal average of the fluorescence intensity of one endocytic event. We calculated the linear density of endocytic events as the ratio between the number of endocytic events in a cell and its length.

Measurement of eisosomes' density on the plasma membrane

We imaged full cells expressing Pil1p-mEGFP by taking stacks of 0.5-µm spaced Z-slices. We corrected these Z-stacks for uneven illumination and manually outlined individual cells to determine the surface area of each cell. To determine the total amount of eisosome-bound Pil1p-mEGFP we subtracted the cytosolic intensity of Pil1-mEGFP using a pre-determined threshold and summed all the Z-slices. We measured the mean membrane intensity of each cell on the thresholded sum-projection image. The eisosome density was determined by dividing this mean intensity by the surface area of each protoplast.

Measurement of membrane tension

Protoplasts were loaded in a custom-built chamber which was passivated with 0.2 mg/mL β-casein (Millipore-Sigma, Saint-Louis, USA) for 30 minutes and pre-equilibrated with EMM5S supplemented with 0.8 M D-Sorbitol. A glass micropipette (#1B100-4, World Precision Instruments, Sarasota, USA) was forged to a diameter smaller than the average protoplast radius (~2.5 µm), and was connected to a water reservoir of adjustable height to apply a defined aspiration pressure. Before and after each experiment the height of the water reservoir was adjusted to set the aspiration pressure to 0. Cells were imaged with a bright field IX-71 inverted microscope (Olympus, Tokyo, Japan) equipped with a 60X/1.4NA objective, and images were recorded every second. Aspiration pressure was gradually increased every 30 s and the membrane tension σ was calculated as $\sigma = \Delta P.R_p/[2(1 - R_p/R_c)]$, where R_p and R_c are respectively the micropipette and the cell radius, ΔP is the aspiration pressure for which the length of the tongue l of the protoplast in the micropipette is equal to R_p [40]. To limit the effects of the adaptation of cells' membrane tension, all measurements were performed within the first five minutes after the hypotonic shock, which greatly limited the throughput of our assay (1 measurement per sample), compared to the measurements at steady state (around 6 measurements per sample).

Acknowledgements

We thank Yale West Campus Imaging core for providing access to the spinning disc confocal microscope, members of the Berro lab for insightful discussions and R. Fernandez for providing mutant yeast strains. We thank Ramesh Ramji and Kathryn Miller-Jensen for initial help with the microfluidics part of this project. We gratefully thank Millipore Sigma for lending us a CellASIC unit and Erdem Karatekin for access to his micropipette aspiration setup. We also thank Samantha Dundon, Mike Lacy and Matt Akamatsu for their comments on our manuscript. This research was supported in part by National Institutes of Health/National Institute of General Medical Sciences Grant R01GM115636 and by seed funding from the American Cancer Society Institutional Research Grant #IRG 58-012-58.

References

1. Schaber, J. *et al.* Biophysical properties of Saccharomyces cerevisiae and their relationship with HOG pathway activation. *Eur. Biophys. J.* **39,** 1547–1556 (2010).
2. Minc, N., Boudaoud, A. & Chang, F. Mechanical forces of fission yeast growth. *Curr. Biol.* **19,** 1096–1101 (2009).
3. Dmitrieff, S. & Nédélec, F. Membrane Mechanics of Endocytosis in Cells with Turgor. *PLoS Comput. Biol.* **11,** (2015).
4. Aghamohammadzadeh, S., Smaczynska-de Rooij, I. I. & Ayscough, K. R. An Abp1-dependent route of endocytosis functions when the classical endocytic pathway in yeast is inhibited. *PLoS One* **9,** (2014).
5. Basu, R., Munteanu, E. L. & Chang, F. Role of turgor pressure in endocytosis in fission yeast. *Mol. Biol. Cell* **25,** 679–87 (2013).
6. Carlsson, A. E. & Bayly, P. V. Force generation by endocytic actin patches in

budding yeast. *Biophys. J.* **106,** 1596–1606 (2014).
7. Palmer, S. E. *et al.* A dynamin-actin interaction is required for vesicle scission during endocytosis in yeast. *Curr. Biol.* **25,** 868–878 (2015).
8. Aghamohammadzadeh, S. & Ayscough, K. R. Differential requirements for actin during yeast and mammalian endocytosis. *Nat. Cell Biol.* **11,** 1039–1042 (2009).
9. Boulant, S., Kural, C., Zeeh, J.-C., Ubelmann, F. & Kirchhausen, T. Actin dynamics counteract membrane tension during clathrin-mediated endocytosis. *Nat. Cell Biol.* **13,** 1124–1131 (2011).
10. Hassinger, J. E., Oster, G., Drubin, D. G. & Rangamani, P. Design principles for robust vesiculation in clathrin-mediated endocytosis. *Proc. Natl. Acad. Sci.* **114,** E1118–E1127 (2017).
11. Ferguson, S. *et al.* Coordinated Actions of Actin and BAR Proteins Upstream of Dynamin at Endocytic Clathrin-Coated Pits. *Dev. Cell* **17,** 811–822 (2009).
12. Hohmann, S. An integrated view on a eukaryotic osmoregulation system. *Curr. Genet.* **61,** 373–382 (2015).
13. Hohmann, S. Osmotic Stress Signaling and Osmoadaptation in Yeasts Osmotic. *Microbiol. Mol. Biol. Rev.* **66,** 300–372 (2002).
14. Suescún-Bolívar, L. P. & Thomé, P. E. Osmosensing and osmoregulation in unicellular eukaryotes. *World J. Microbiol. Biotechnol.* **31,** 435–443 (2015).
15. Atilgan, E., Magidson, V., Khodjakov, A. & Chang, F. Morphogenesis of the Fission Yeast Cell through Cell Wall Expansion. *Curr. Biol.* **25,** 2150–7 (2015).
16. Sinha, B. *et al.* Cells respond to mechanical stress by rapid disassembly of caveolae. *Cell* **144,** 402–413 (2011).
17. Kabeche, R., Howard, L. & Moseley, J. B. Eisosomes provide membrane reservoirs for rapid expansion of the yeast plasma membrane. *J. Cell Sci.* **128,** 4057–4062 (2015).
18. Berro, J. & Pollard, T. D. Local and global analysis of endocytic patch dynamics in fission yeast using a new ‘temporal superresolution’ realignment method. *Mol. Biol. Cell* **25,** 3501–14 (2014).
19. Berro, J. & Pollard, T. D. Synergies between Aip1p and capping protein subunits (Acp1p and Acp2p) in clathrin-mediated endocytosis and cell polarization in fission yeast. *Mol. Biol. Cell* **25,** 3515–27 (2014).
20. Skau, C. T. *et al.* Actin filament bundling by fimbrin is important for endocytosis, cytokinesis, and polarization in fission yeast. *J. Biol. Chem.* **286,** 26964–77 (2011).
21. Sirotkin, V., Berro, J., Macmillan, K., Zhao, L. & Pollard, T. D. Quantitative analysis of the mechanism of endocytic actin patch assembly and disassembly in fission yeast. *Mol. Biol. Cell* **21,** 2894–904 (2010).
22. Sens, P. & Turner, M. S. Budded membrane microdomains as tension regulators. *Phys. Rev. E - Stat. Nonlinear, Soft Matter Phys.* **73,** 1–4 (2006).
23. Lo, H. P., Hall, T. E. & Parton, R. G. Mechanoprotection by skeletal muscle caveolae. *Bioarchitecture* **0992,** 00–00 (2016).
24. Cheng, J. P. X. *et al.* Caveolae protect endothelial cells from membrane rupture during increased cardiac output. *J. Cell Biol.* **211,** 53–61 (2015).
25. Kabeche, R., Baldissard, S., Hammond, J., Howard, L. & Moseley, J. B. The filament-forming protein Pil1 assembles linear eisosomes in fission yeast. *Mol. Biol. Cell* **22,** 4059–4067 (2011).
26. Olivera-Couto, A., Grana, M., Harispe, L. & Aguilar, P. S. The eisosome core is composed of BAR domain proteins. *Mol. Biol. Cell* **22,** 2360–2372 (2011).

27. Ziółkowska, N. E., Karotki, L., Rehman, M., Huiskonen, J. T. & Walther, T. C. Eisosome-driven plasma membrane organization is mediated by BAR domains. *Nat. Struct. Mol. Biol.* **18,** 854–856 (2011).
28. Flor-Parra, I., Zhurinsky, J., Bernal, M., Gallardo, P. & Daga, R. R. A Lallzyme MMX-based rapid method for fission yeast protoplast preparation. *Yeast* **31,** 61–66 (2014).
29. Stachowiak, M. R. *et al.* Mechanism of cytokinetic contractile ring constriction in fission yeast. *Dev. Cell* **29,** 547–61 (2014).
30. Lacy, M. M., Baddeley, D. & Berro, J. Single-molecule imaging of the BAR-domain protein Pil1p reveals filament-end dynamics. *Mol. Biol. Cell* **28,** 2251–2259 (2017).
31. Burke, T. A. *et al.* Homeostatic actin cytoskeleton networks are regulated by assembly factor competition for monomers. *Curr. Biol.* **24,** 579–585 (2014).
32. Ferguson, J. P. *et al.* Mechanoregulation of clathrin-mediated endocytosis. *J. Cell Sci.* **130,** 3631–3636 (2017).
33. Mostov, K. E., Verges, M. & Altschuler, Y. Membrane traffic in polarized epithelial cells. *Curr. Opin. Cell Biol.* **12,** 483–490 (2000).
34. Urbina, F. L., Gomez, S. M. & Gupton, S. L. Spatiotemporal organization of exocytosis emerges during neuronal shape change. *J. Cell Biol.* **217,** 1113–1128 (2018).
35. Watanabe, S. & Boucrot, E. Fast and ultrafast endocytosis. *Curr. Opin. Cell Biol.* **47,** 64–71 (2017).
36. Nicholson-Fish, J. C., Smillie, K. J. & Cousin, M. A. Monitoring activity-dependent bulk endocytosis with the genetically-encoded reporter VAMP4-pHluorin. *J. Neurosci. Methods* **266,** 1–10 (2016).
37. Schindelin, J. *et al.* Fiji: An open-source platform for biological-image analysis. *Nature Methods* **9,** 676–682 (2012).
38. Schneider, C. A., Rasband, W. S. & Eliceiri, K. W. NIH Image to ImageJ: 25 years of image analysis. *Nat. Methods* **9,** 671–675 (2012).
39. Tinevez, J. Y. *et al.* TrackMate: An open and extensible platform for single-particle tracking. *Methods* **115,** 80–90 (2017).
40. Evans, E. & Yeung, a. Apparent viscosity and cortical tension of blood granulocytes determined by micropipet aspiration. *Biophys. J.* **56,** 151–160 (1989).

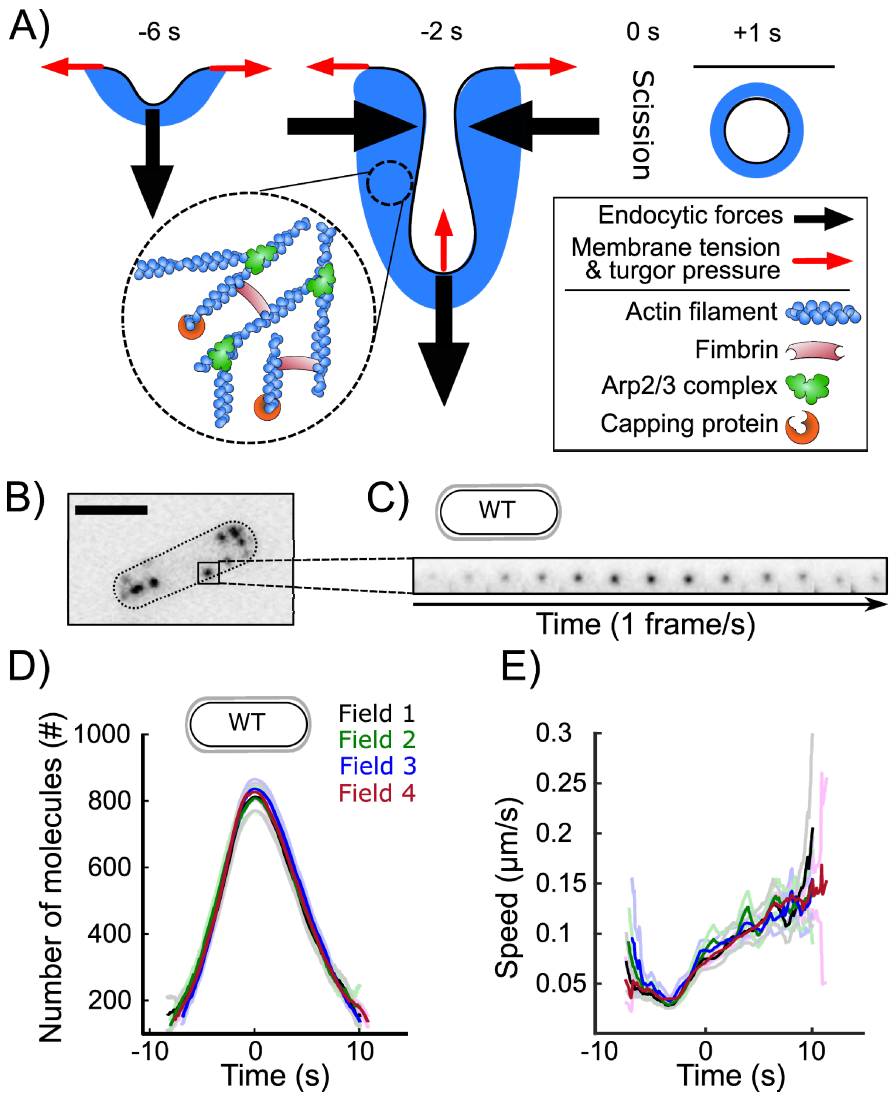

Figure 1: Quantitative measurements of fimbrin dynamics at sites of clathrin-mediated endocytosis are highly reproducible. A) Schematic of the plasma membrane deformations and the main components of the actin machinery during CME. Fimbrin (Fim1p, red) crosslinks actin filaments (blue) present at endocytic sites. B) Wild-type yeast cell expressing Fim1p-mEGFP (inverted contrast). Scale bar = 5 µm. C) Montage of a representative CME event. The interval between each frame is 1 s. D) and E) The number of molecules (D) and speed (E) of Fim1p-mEGFP detected, tracked and aligned with temporal super-resolution (Berro & Pollard, 2014) is highly reproducible between fields of view. Each curve with a dark color represents the average of several endocytic events from a different field of view of the same sample (black: N=64; green: N=79; blue: N=91; purple: N=202), and the light colors are the 95% confidence intervals. For each average curve, the peak value corresponds to time 0 sec, when vesicles scission happens.

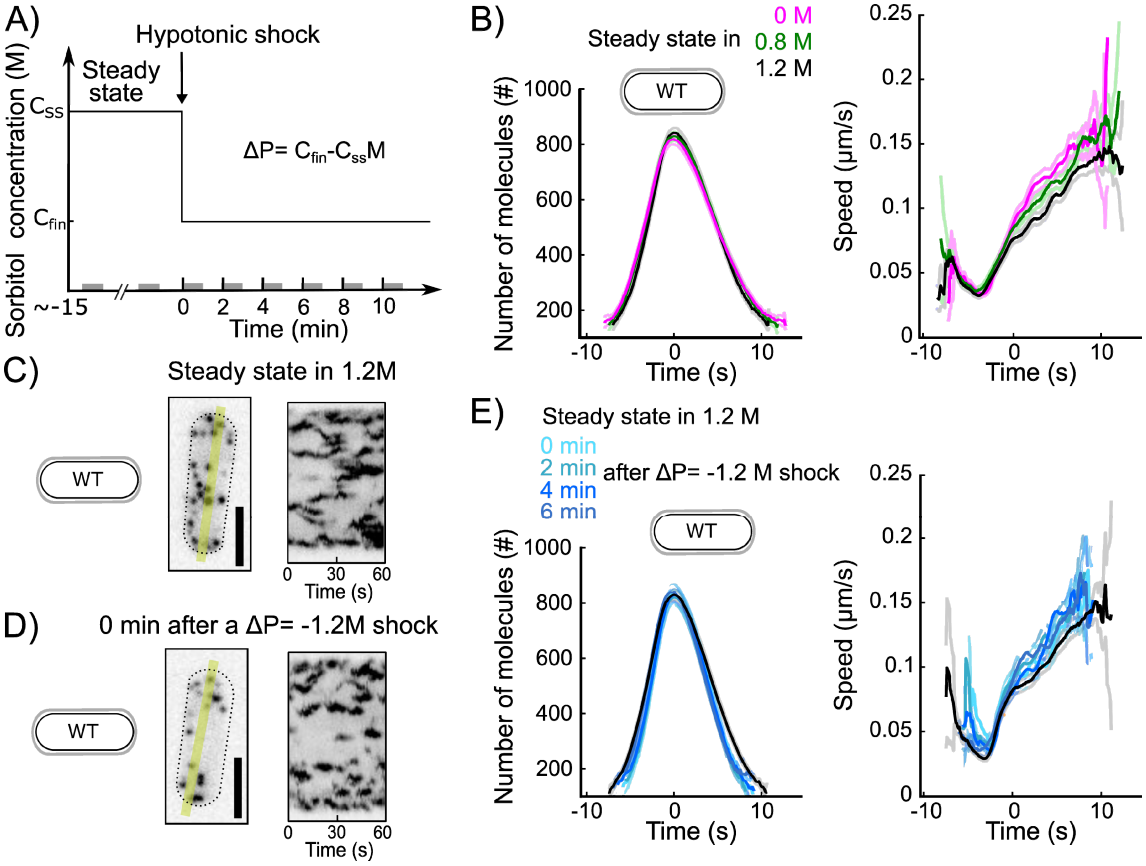

Figure 2: CME in wild-type walled cells is robust over a wide range of osmotic conditions. A) Timeline of the experiments and notations. By convention, hypotonic shocks start at time 0 min and are defined by the difference in concentration of sorbitol in the steady state media before the shock (C_{SS}) and after the hypotonic shock (C_{fin}), $\Delta P = C_{fin} - C_{SS}$. In the figures of this paper, data for a given time point correspond to endocytic events happening within 1 minute after this time point (e.g. the data at t=0 min correspond to endocytic events happening between 0 and 1 min after the shock). These time intervals are represented by gray bars on the time axis. B) Number of molecules (left panel) and speed (right panel) of Fim1p-mEGFP in wild-type walled cells at steady state in media supplemented with different sorbitol concentrations. Fuschia: 0 M (N=388); green: 0.8 M (N=454); black: 1.2 M (N=451). C) and D) Left panels: representative wild-type walled cells expressing Fim1p-mEGFP (inverted contrast) at steady state in 1.2 M sorbitol (C) and immediately (0 min) after an acute osmotic shock ΔP=-1.2 M (D). Right panels: kymographs of the fluorescence under the yellow line in the left panels. Black dashed lines: outline of the cell. Scale bars for all panels: 5 µm. E) Number of molecules (left panel) and speed (right panel) of Fim1p-mEGFP for wild-type walled cells initially at steady state in 1.2 M sorbitol and after an acute osmotic shock of ΔP=-1.2 M. Black: steady state in 1.2 M sorbitol (N=354); light to dark blue in top panel: 0 min (N=103), 2 min (N=169), 4 min (N=190), and 6 min (N=153) after the acute hypotonic shock. (B) and (E): dark colors: average; light colors: average +/- 95% confidence interval.

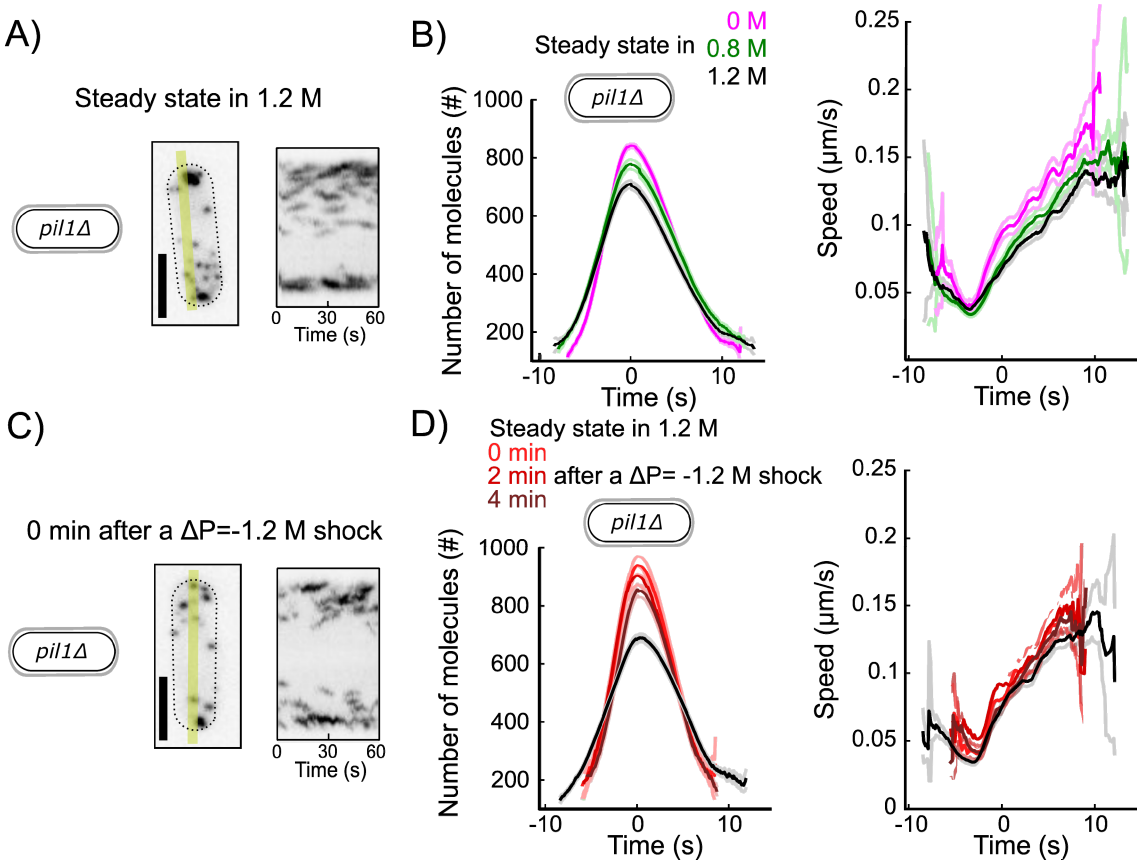

Figure 3: The absence of eisosome makes the dynamics of the CME machinery more sensitive to changes in osmoloarity. A) and C) Left panels: representative *pil1Δ* walled cells expressing Fim1p-mEGFP (inverted contrast) at steady state in 1.2 M sorbitol (A) and immediately (0 min) after an acute osmotic shock of ΔP=-1.2 M (C). Right panels: kymographs of the fluorescence under the yellow lines in the left panels. Black dashed lines: cell outline. Scale bars: 5 µm. B) Number of molecules (left panel) and speed (right panel) of Fim1p-mEGFP in *pil1Δ* walled cells at steady state in media supplemented with different sorbitol concentrations. Purple: 0 M (N=342); green: 0.8 M (N=516); black: 1.2 M (N=514). D) Number of molecules (left panel) and speed (right panel) of Fim1p-mEGFP in *pil1Δ* walled cells before and after an acute osmotic shock (ΔP=-1.2 M). Black: steady state in 1.2 M sorbitol before the hypotonic shock (N=583); light to dark red in top panel: 0 min (N=176), 2 min (N=145) and 4 min (N=326) after the acute hypotonic shock. (B) and (D): dark colors: average; light colors: average +/- 95% confidence interval.

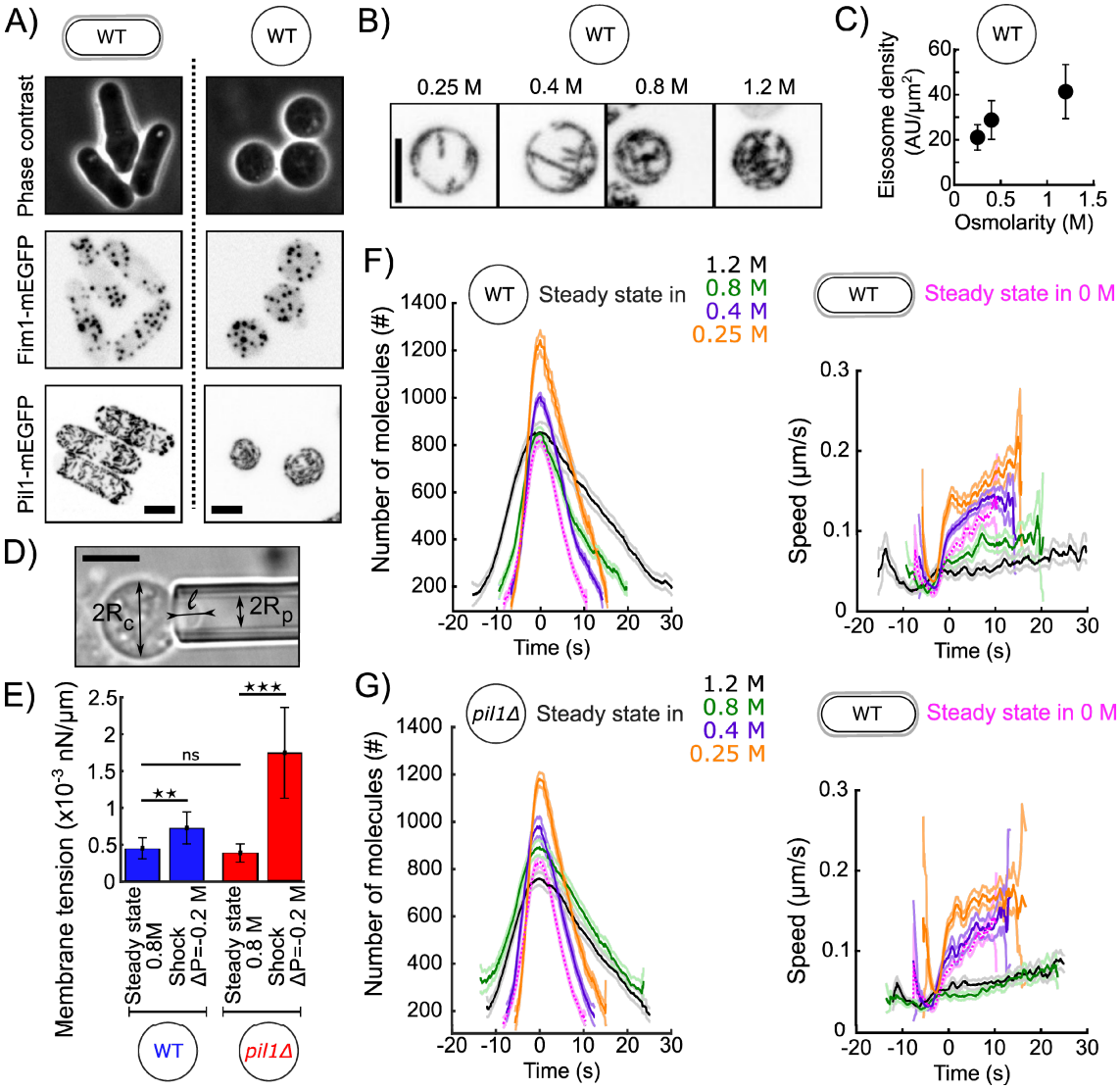

Figure 4: Eisosomes buffer increases in membrane tension but has virtually no influence on the dynamics of the actin endocytic machinery at steady state in protoplasts. A) Representative walled yeast cells (left column) and protoplasts (right column) at steady state in 1.2 M sorbitol. Top panels: phase contrast; middle panels: cells expressing Fim1-mEGFP (inverted contrast); bottom panels: cells expressing Pil1-mEGFP (inverted contrast). B) Eisosomes labelled with Pil1p-GFP (inverted contrast) in wild-type protoplasts at steady state in different sorbitol concentrations. From left to right: 0.25 M, 0.4 M, 0.8 M and 1.2 M sorbitol. C) Density of eisosomes at the plasma membrane, measured as the ratio between the intensity of Pil1p-GFP on the plasma membrane and the surface area of the protoplast, at steady state in 0.25 M (N=26), 0.4 M (N=34) and 1.2 M (N=39) sorbitol. Error bars: standard deviations. D) Micropipette aspiration was used to measure membrane tension. R_c: cell radius; R_p: micropipette radius; l: length of the tongue inside the micropipette. E) Membrane tension of protoplasts at steady state in 0.8 M sorbitol and ~ 5 min after a hypotonic shock (ΔP=-0.2 M) for wild type (blue bars, N=28 for steady state and N=5 for the shock) and *pil1Δ* protoplasts (red bars, N=42 for steady state and N=7 for the shock). p-values: non-significant (ns), $p>0.05$; two stars (**), $p\leq0.01$; three stars (***), $p\leq0.001$. F) and G) Number of molecules (left panels) and speed (right panels) of Fim1p-mEGFP

for WT (F) and *pil1Δ* (G) protoplasts at steady state in different sorbitol concentrations. Orange: 0.25 M (N_{WT}=395, $N_{pil1\Delta}$=370); purple: 0.4 M (N_{WT}=682, $N_{pil1\Delta}$=166); green: 0.8 M (N_{WT}=151, $N_{pil1\Delta}$=184); black: 1.2 M (N_{WT}=143, $N_{pil1\Delta}$=203). Dark colors: average; light colors: average +/- 95% confidence interval. Fuschia dotted curves: wild-type walled cells at steady state in 0 M sorbitol (same as Figure 3B). (A), (B) and (D), scale bars: 5 µm.

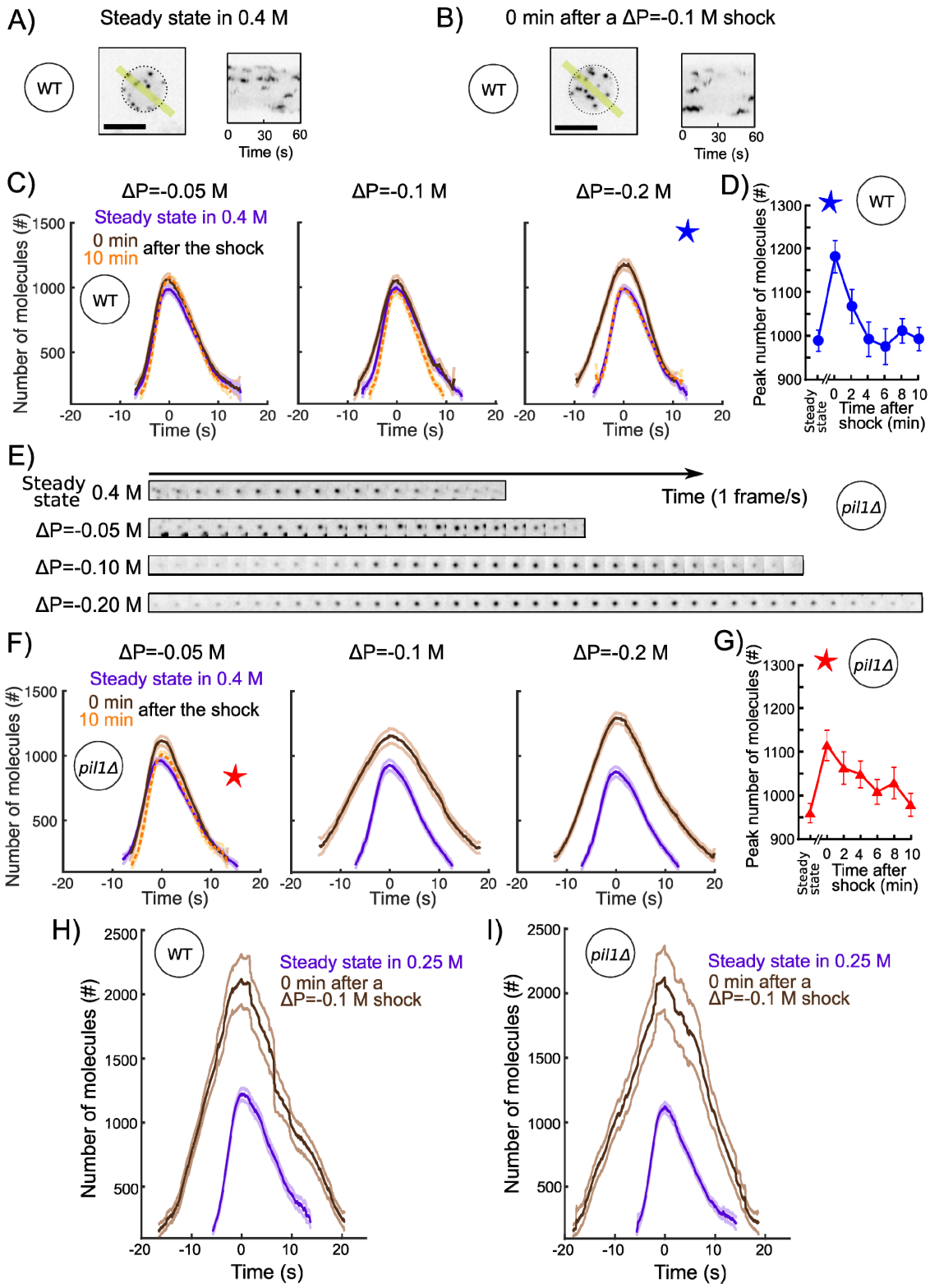

Figure 5: The actin endocytic machinery adapts to increases of membrane tension in protoplasts. A) and B) Representative wild-type protoplasts expressing Fim1-mEGFP (inverted contrast) at steady-state in 0.25 M sorbitol (A, left panel) and immediately after (0 min) an acute osmotic shock of ΔP=-0.1 M (B, left panel). Right

panels: kymographs of the fluorescence under the yellow lines in the left panels. Black dashed lines: protoplast outline. Scale bars: 5 µm. C) and F) Number of Fim1p-mEGFP molecules in wild type (C) and *pil1Δ* (F) protoplasts at steady-state in 0.4 M sorbitol (purple dashed, N_{WT}=279, 413, 269 and $N_{pil1\Delta}$=429, 95, 95), 0 min (brown, N_{WT}=193, 190, 396 and $N_{pil1\Delta}$=183, 215, 373) and 10 min (orange line, N_{WT}=182, 186, 309 and $N_{pil1\Delta}$=206) after an hypotonic shock of ΔP=-0.05 M (left panels), ΔP=-0.1 M (middle panels) and ΔP=-0.2 M (right panels). Note that the large majority of *pil1Δ* protoplasts were too damaged or dead 2 minutes after hypotonic shocks of ΔP=-0.1 M or larger to allow us to track enough endocytic events and produce a curve (Supplemental Figure S7). D) Temporal adaptation of the peak number of Fim1p-mEGFP in wild type protoplasts initially at steady state in 0.4 M sorbitol and 0 to 10 min after a ΔP=-0.2 M osmotic shock. The condition for this figure is the same as the condition with the blue star in (C). E) Montage of representative endocytic events (Fim1-mEGFP, inverted contrast) in *pil1Δ* protoplasts (1 frame per second) at steady state in 0.4 M sorbitol (first row) and immediately after (0 min) a hypotonic shocks of ΔP=-0.05 M (second row), ΔP=-0.10 M (third row) and ΔP=-0.20 M (fourth row). G) Same as (D) but for *pil1Δ* protoplasts after a ΔP=-0.05 M shock. The condition in this figure is the same as the condition with the red star in F. (D) and (G) error bars are 95% confidence intervals. H) and I) Number of molecules of Fim1p-mEGFP for WT (H) and *pil1Δ* (I) protoplasts at steady state in 0.25 M sorbitol (purple dashed, N_{WT}=226 and $N_{pil1\Delta}$=182) and immediately after (0 min) a hypotonic shock of ΔP=-0.1 M (brown, N_{WT}=75 and $N_{pil1\Delta}$=67).

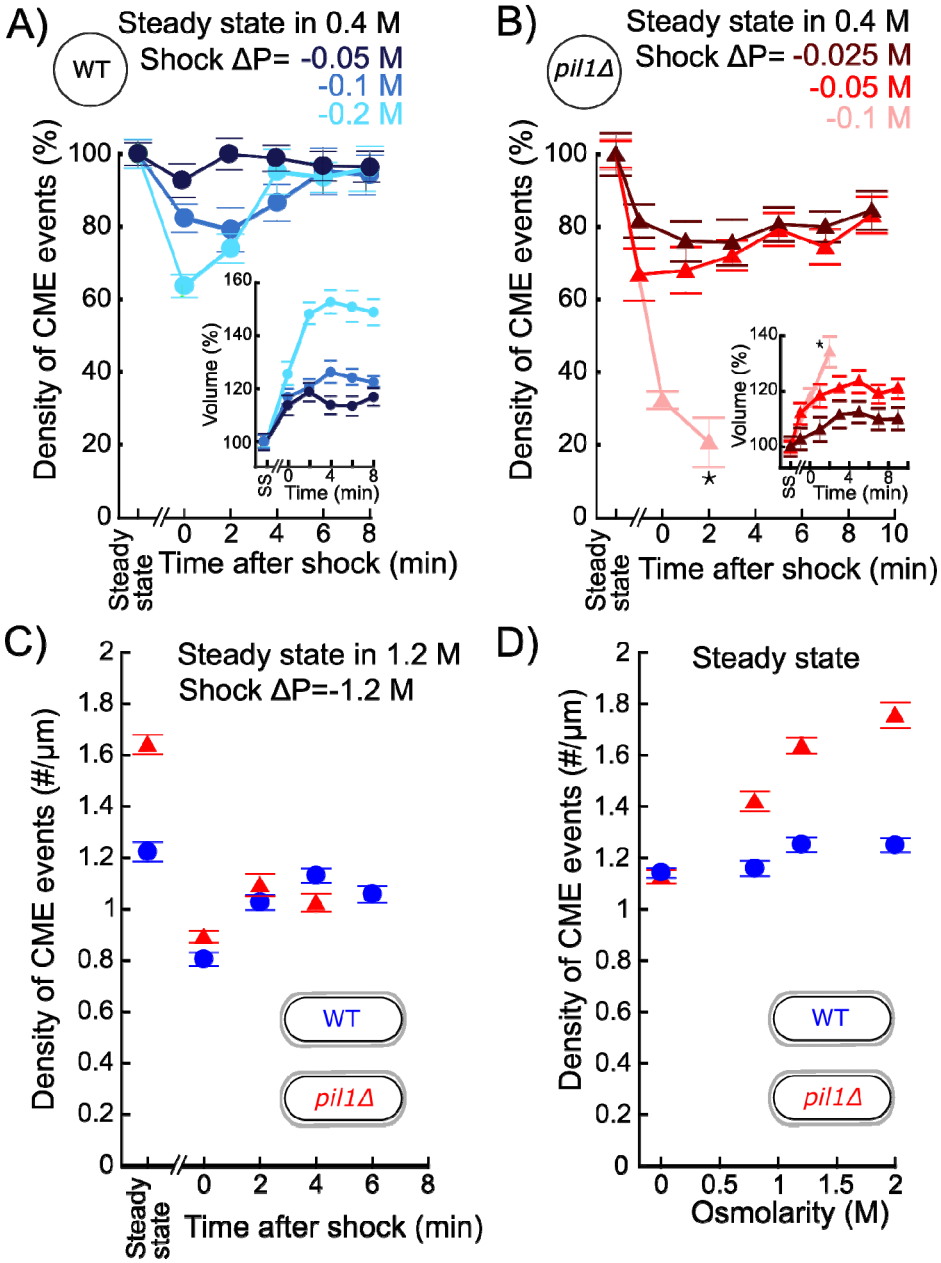

Figure 6: The density of endocytic events rapidly adapts after acute osmotic shocks. A) Temporal evolution of density of endocytic events (average number of endocytic events at a given time in a cell divided by the cell length) in wild type protoplasts initially at steady state in 0.4 M sorbitol and after an acute hypotonic shock of ΔP=-0.05 M (dark blue, N_{SS}=172, N_{0min}=102, N_{2min}=117, N_{4min}=114, N_{6min}=113, N_{8min}=124), ΔP=-0.1M (blue, N_{SS}=127, N_{0min}=62, N_{2min}=70, N_{4min}=78, N_{6min}=62, N_{8min}=54) and ΔP=-0.2M (light blue, N_{SS}=146, N_{0min}=149, N_{2min}=158, N_{4min}=83, N_{6min}=107, N_{8min}=83). B) Same as (A) but with *pil1Δ* protoplasts and hypotonic shocks of ΔP=-0.025 M (dark red, N_{SS}=99, N_{0min}=100, N_{2min}=71, N_{4min}=70, N_{6min}=98, N_{8min}=118, N_{10min}=96), ΔP=-0.05 M (red, N_{SS}=263, N_{0min}=106, N_{2min}=111, N_{4min}=106, N_{6min}=103, N_{8min}=123, N_{10min}=104) and ΔP=-0.1 M (light red, N_{SS}=151, N_{0min}=125, N_{2min}=78). (A) and (B) insets: relative volume increase after the hypotonic shocks (the volume at steady state is used as a reference). The number of cells measured in the

insets are the same as in the main figures. Star (*): the large majority of *pil1Δ* protoplasts were too damaged or dead 4 minutes after the hypotonic shocks at ΔP=-0.1 M, which prevented us from measuring the density of endocytic events and the volume after this time point. C) Density of endocytic events in wild-type (blue circle) and *pil1⊿* (red triangle) walled cells initially at steady state in 1.2 M sorbitol and after an acute hypotonic shock of ΔP=-1.2M (Wild-type: N_{SS}=62, N_{0min}=82, N_{2min}=77, N_{4min}=67, N_{6min}=66; *pil1⊿*: N_{SS}=119, N_{0min}=69, N_{2min}=44, N_{4min}=67. D) Density of endocytic events in intact cells at steady state in different osmolarities. (Wild-type: N_{0M}=240, $N_{0.8M}$=103, $N_{1.2M}$=159, N_{2M}=161; *pil1⊿*: N_{0M}=188, $N_{0.8M}$=105, $N_{1.2M}$=183, N_{2M}=80). (A), (B), (D) and (E): error bars are standard errors of the mean.

Supplemental figures

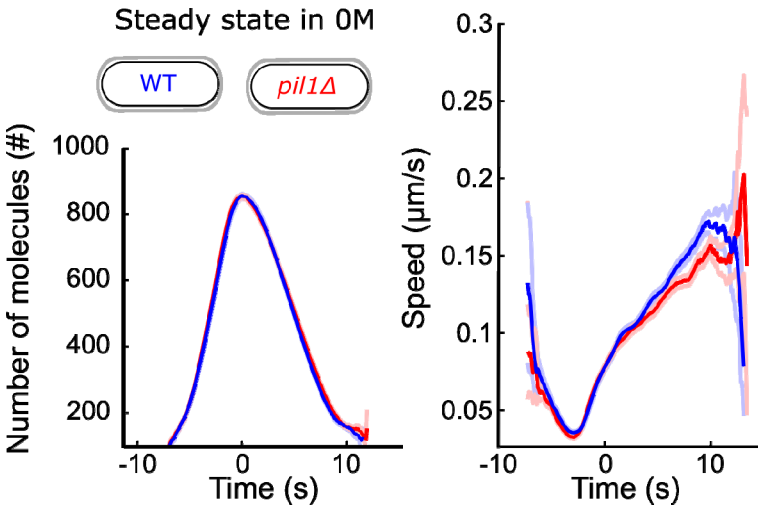

Supplemental Figure S1 (complementing Figure 3): The number of molecules (left panel) and speed (right panel) of Fim1p-mEGFP at CME sites in wild-type (blue, N=1773) and *pil1Δ* (red, N=1884) walled cells at steady state in EMM5S without sorbitol are identical (same data as Figures 2B and 3B). Dark colors: average, light colors: average +/- 95% confidence interval.

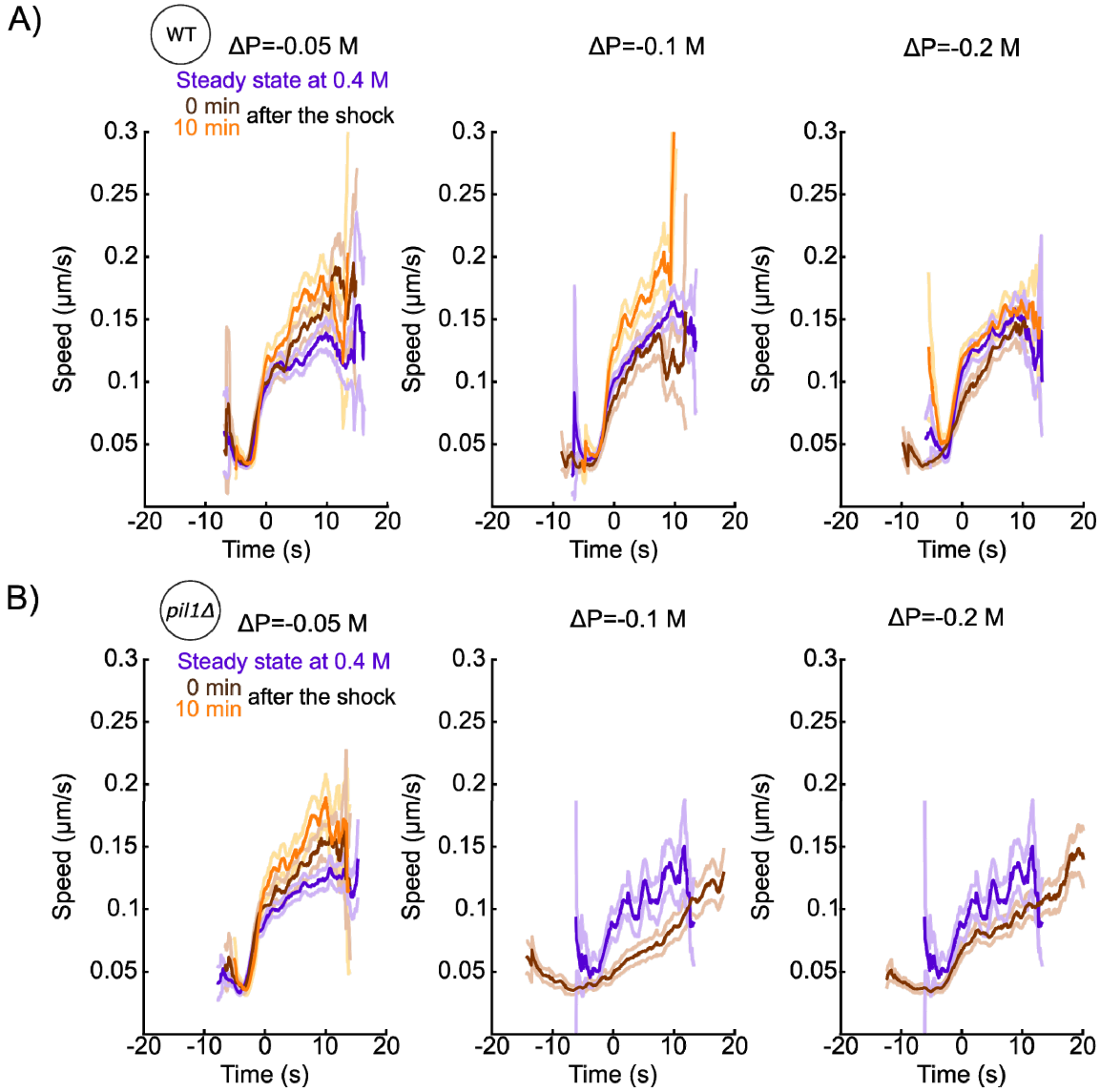

Supplemental Figure S2 (complementing Figures 5B and 5D): Speed of Fim1p-mEGFP in wild type (A) and *pil1Δ* (B) protoplasts at steady-state in 0.4 M sorbitol (purple, N_{WT}=279, 413, 269 and $N_{pil1\Delta}$=429, 95, 95 for ΔP=-0.05 M, -0.1 M and -0.2 M respectively), 2 minutes (brown, N_{WT}=193, 190, 396 and $N_{pil1\Delta}$=183, 215, 373) and 10 minutes (orange, N_{WT}=182, 186, 309 and $N_{pil1\Delta}$=206) after a hypotonic shock of ΔP=-0.05 M (left panels), ΔP=-0.1 M (middle panels) and ΔP=-0.2 M (right panels). Dark colors: average, light colors: average +/- 95% confidence interval, N_{WT} and $N_{pil1\Delta}$ are given from low to high osmotic shocks.

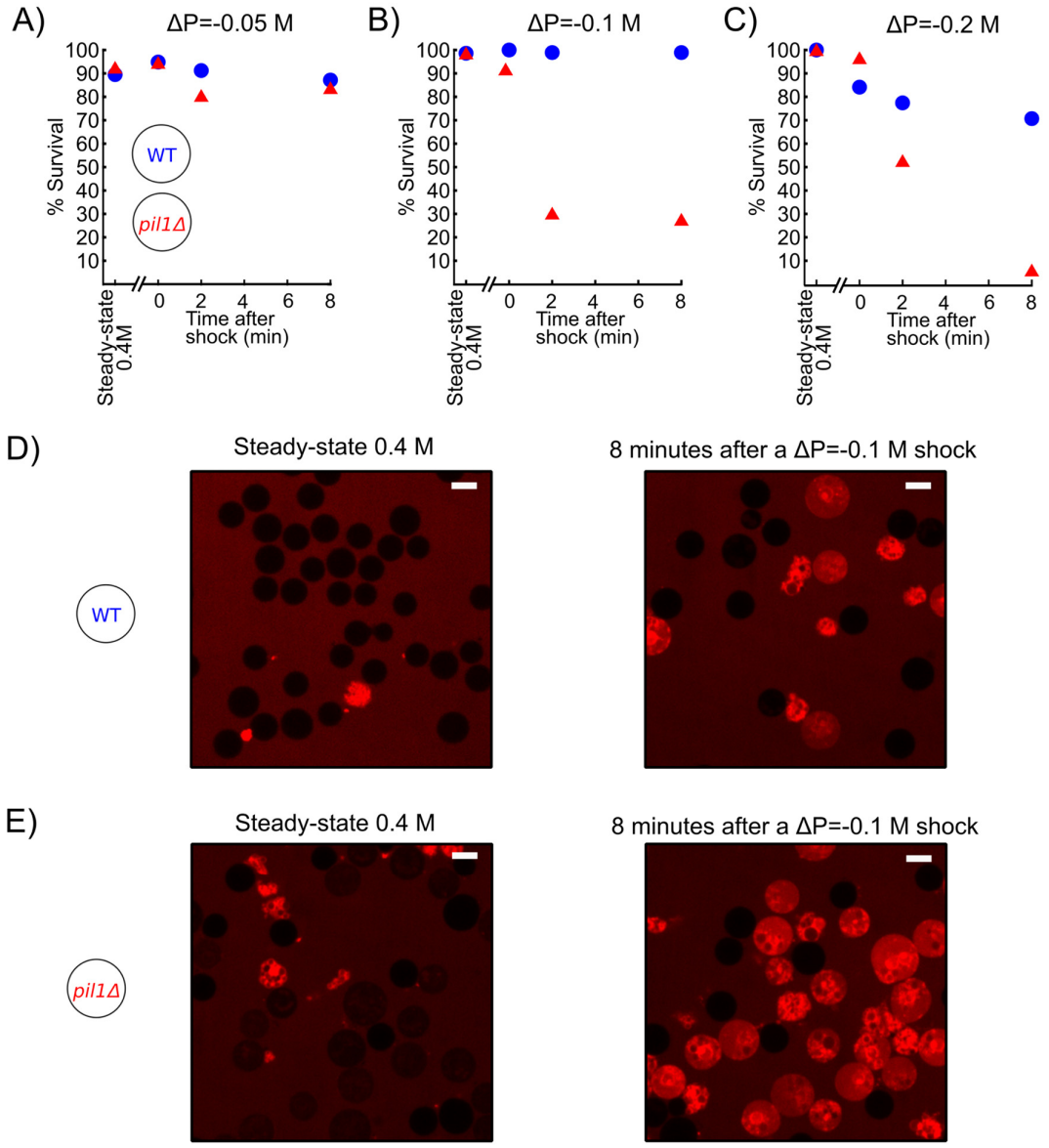

Supplemental Figure S3 (complementing Figures 5B and 5D): Percentage of wild-type (blue dots) and *pil1Δ* (red triangle) protoplasts that are alive in fields of view used for analysis, at steady-state in 0.4 M sorbitol, and after a ΔP=-0.05 M (A), ΔP=-0.1 M (B) and ΔP=-0.2 M (C) hypotonic shocks. D) and E) Typical fields of view of wild-type (D) and *pil1Δ* (E) protoplasts at steady state in 0.4 M sorbitol (left panel) and 8 minutes (right panel) after a ΔP=-0.1 M hypotonic shock. Cells are considered alive if they do not contain any red fluorescence from the sulforhodamin B dye. Scale bar: 5 µm.

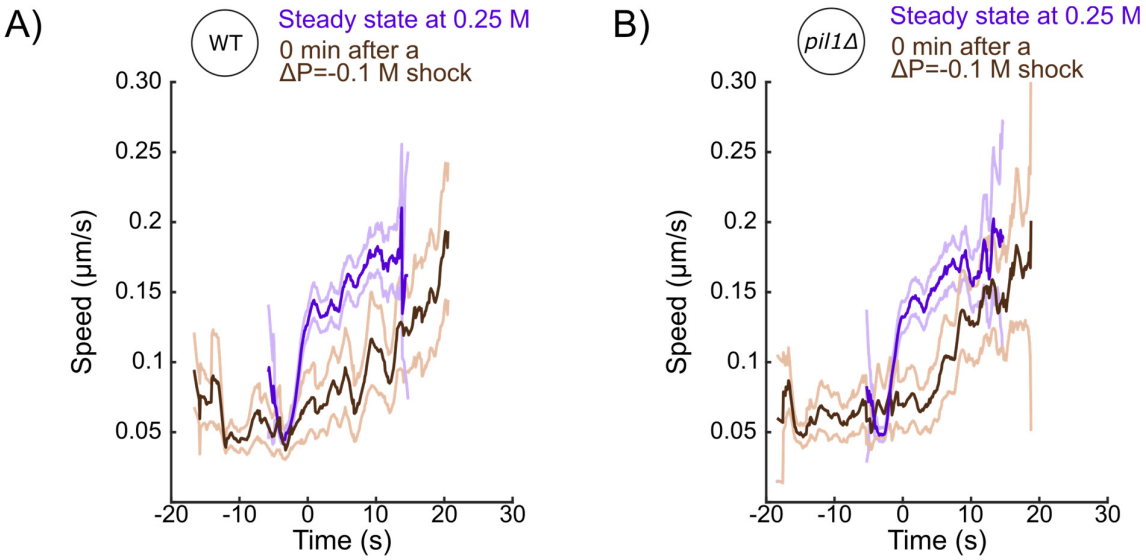

Supplemental Figure S4 (complementing Figures 5H and 5I): Speed of Fim1p-mEGFP at CME sites for WT (A) and *pil1Δ* (B) protoplasts at steady-state in 0.25 M sorbitol (purple; N_{WT}=226, $N_{pil1\Delta}$=182) and immediately (0 min) after (brown; N_{WT}=67, $N_{pil1\Delta}$=75) a hypotonic shock of ΔP=-0.1 M. Dark colors: average, light colors: average +/- 95% confidence interval.

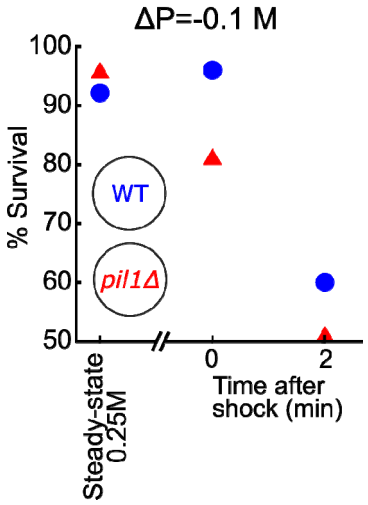

Supplemental Figure S5 (complementing Figures 5H and 5I): Percentage of wild-type (blue dots) and *pil1Δ* (red triangle) protoplasts that are alive in fields of view used for analysis, at steady-state in 0.25 M sorbitol, and after a ΔP=-0.1 M hypotonic shock.

Supplemental Table 1: Yeast strains

Yeast Name	Genotype	Mating type
SpJB57	fim1-mEGFP-NatMX6 ade6-M216 his3-Δ1 leu1-32 ura4-Δ18	h+
SpJB234	pil1Δ fim1-mEGFP-NatMX6 ade6-M216 his3-Δ1 leu1-32 ura4-Δ18	h-
SpJB204	pil1-mEGFP-kanMX6 ade6-M216 his3-Δ1 leu1-32 ura4-Δ18	h-